scientific reports

Check for updates

OPEN

Direct NO_2 formation from N_2-O_2 supercritical fluid plasma

Juho Lee[1], Kyusang Cho[1], Seungjun Lee[2] & Gunsu Yun[1,2]✉

We demonstrate a novel approach for the direct formation of nitrogen dioxide (NO_2) in a supercritical nitrogen–oxygen mixture using laser-produced plasma. By tightly focusing a nanosecond laser pulse into the dense fluid, we generate a high electron density plasma that enables chemical reactions not accessible under ambient conditions. Optical emission and absorption spectroscopy confirm the in-situ formation of NO_2, and parametric investigations reveal that the yield is highly sensitive to the plasma characteristics and gas composition. These findings demonstrate the potential of using plasma as a compact and selective chemical microreactor in dense media, opening new possibilities for on-demand molecular synthesis in extreme environments such as space exploration.

Nitrogen dioxide (NO_2) is a key intermediate in a wide range of industrial and environmental processes[1], including nitric acid synthesis, combustion chemistry, and atmospheric reactions[2,3]. The conventional industrial method for NO_2 production is the Ostwald process, which begins with ammonia (NH_3) oxidation under high temperature in the presence of a catalyst[1,4,5]. While this method is well-established and suitable for large-scale production, this process has inherent limitations, such as dependence on NH_3 feedstock, lack of flexibility for small-scale or decentralized deployment, and the potential emission of environmentally hazardous by-products such as nitrous oxide (N_2O), a greenhouse gas. In addition, the process is strongly dependent on the quality and durability of the catalyst in the oxidation process of ammonia and nitrogen oxides, which can significantly affect efficiency[6–9].

In this context, direct synthesis of NO_2 from molecular nitrogen (N_2) and oxygen (O_2), bypassing the NH_3 -based step, presents a fundamentally distinct and potentially more versatile approach. This route not only simplifies the overall process but also enables NO_x synthesis in environments where conventional infrastructure is unfeasible, such as in space missions or remote terrestrial environments. However, the extreme stability of the N≡N triple bond and the high activation energy required to initiate N_2-O_2 reactions have long hindered the development of viable methods for direct NO_2 production.

Recent developments in the application of supercritical fluids as reactive media have opened novel strategies for activating stable molecules under extreme conditions[10,11]. Supercritical fluids, states of matter achieved beyond a critical temperature and pressure, exhibit unique thermodynamic properties, including gas-like diffusivity and liquid-like density[12,13]. These features enhance molecular transport and increase collision frequencies, ultimately enabling reaction pathways that would otherwise be unfavorable. Owing to these advantages, supercritical fluids have been employed in the deposition of metal nanoparticles with uniform dispersion on solid substrates, often for the fabrication of nanostructured catalysts and metal-decorated carbon-based materials on complex surfaces[14–16]. In the biomedical field, supercritical fluid-assisted synthesis of inorganic and hybrid nanomaterials has gained attention for enabling precise control over particle size and morphology[17]. Supercritical fluids have also demonstrated potential in the formation of hydrocarbon-based nanostructures, such as diamondoids[18,19]. Plasma discharges within these fluids enhance nucleation and growth from simpler precursors. When combined with energetic plasma discharge, supercritical fluids provide a highly reactive environment where high-pressure, high-density conditions promote bond dissociation and subsequent product formation.

In this study, we investigate the direct synthesis of NO_2 via laser-produced plasma generated in high-pressure supercritical mixtures of N_2 and O_2. We present the first experimental evidence that efficient NO_2 formation can be achieved under these conditions, even in the absence of NH_3 precursors. Through time-resolved imaging, optical emission spectroscopy (OES), and absorption spectrum measurements, we quantify the amount of NO_2 generated in a high-pressure chamber. Moreover, we discuss the broader implications of this plasma–supercritical fluid approach, highlighting its potential for implementation in compact, decentralized chemical systems relevant to in-situ resource utilization (ISRU) in space missions.

[1]Department of Physics, Pohang University of Science and Technology, Pohang, Republic of Korea. [2]Division of Advanced Nuclear Engineering, Pohang University of Science and Technology, Pohang, Republic of Korea. ✉email: gunsu@postech.ac.kr

Results

Characterization of laser-produced plasmas generated in supercritical N^2–O^2 mixtures

Plasma formation in a high-pressure supercritical fluid mixture of N_2 and O_2 is investigated using a high-power pulsed laser. The gas mixture, composed of nitrogen and oxygen in an 8:2 ratio, is pressurized to 100 bar. An Nd:YAG laser (1064 nm, 6 ns, 620 mJ) is employed as the pump laser. Following plasma ignition at the laser focal point, the plasma expands in the backward direction, consistent with previous observations of strongly coupled plasmas in supercritical fluids[20]. Time-resolved plasma imaging, shown in Fig. 1, is performed using an intensified CCD (ICCD) camera with a 3 ns gate width, allowing visualization of plasma dynamics on a nanosecond timescale. The expanding plasma is observed over a delay from −10 ns to 0 ns, reaching its maximum emission intensity and volume at 0 ns. At this peak moment, the plasma volume is estimated to be approximately 1.3 mm^3.

Figure 1d shows the optical emission spectrum measured from the laser-produced plasma. The spectrum is acquired using an ICCD-equipped spectrometer with the same nanosecond time resolution as the plasma images. The vertical axis represents the spectral irradiance, which is absolute calibrated using an intensity calibration light source, allowing for quantitative comparison of emission intensities. The plasma generated in the high-density supercritical fluid exhibits strong continuum emission, which closely matches a blackbody radiation continuum. Fitting the spectrum to a blackbody curve yields a plasma temperature of approximately 1 eV, indicating that the plasma rapidly reaches local thermodynamic equilibrium (LTE) due to the high electron density in the medium. Under such conditions, all species within the plasma are thermally equilibrated. This implies that the plasma formed in the supercritical fluid achieves a localized state of high energy density, providing an ideal environment for driving subsequent chemical reactions, which will be discussed in the following sections.

Direct formation of nitrogen dioxide

During continued plasma generation in the high-pressure supercritical fluid, the initially transparent chamber gradually turns reddish-brown after approximately 10 min (Fig. 2a,b). Notably, this discoloration of the medium persists even after plasma generation stops, indicating the stable formation of colored species. This visual change signifies plasma-driven chemical reactions within the medium, attributed to the formation of nitrogen dioxide NO_2. The presence of NO_2 is supported by its characteristic reddish-brown color, toxic odor, and the appearance of absorption bands in the plasma emission spectrum (Fig. 2c). In the early stages of plasma generation, the emission spectrum resembles blackbody radiation; however, as plasma generation continues, the overall intensity gradually decreases due to absorption. The absorption features appear at wavelengths where NO_2 exhibits a strong absorption cross-section, providing spectroscopic confirmation of its formation.

Given the clearly observed absorption features, the density of the generated NO_2 can be estimated using the Beer–Lambert law:

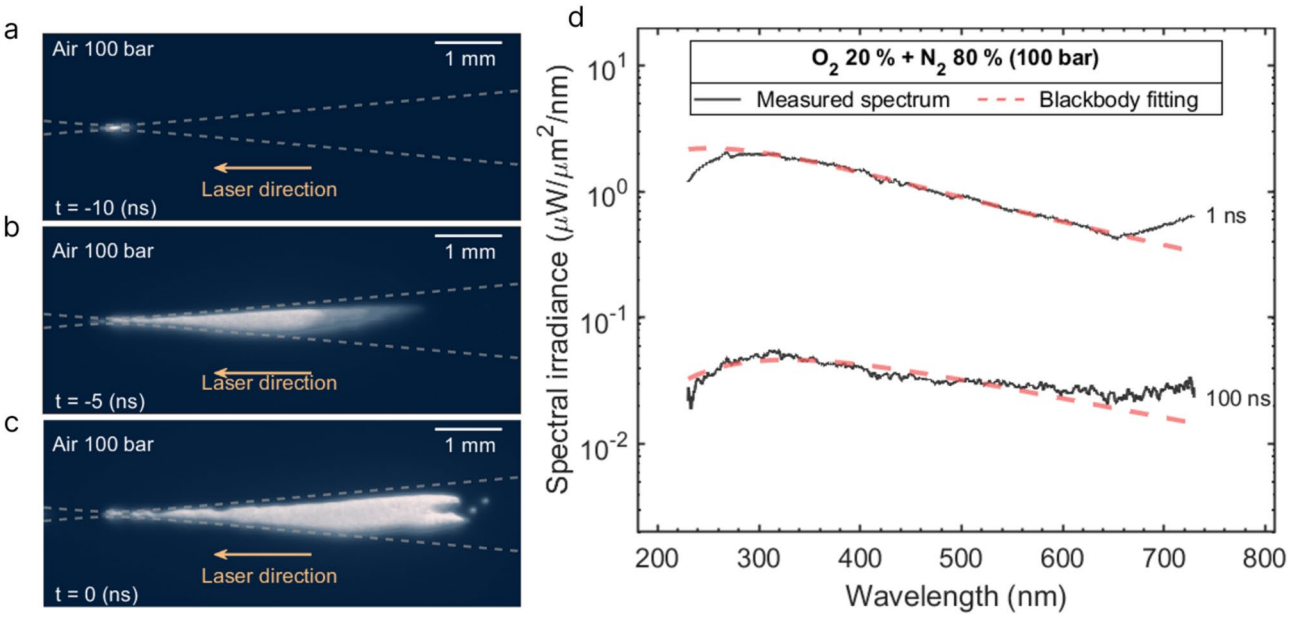

Fig. 1. Time-resolved plasma imaging and OES of laser-produced plasma in a supercritical O_2–N_2 mixture. (**a**–**c**) A plasma is ignited near the laser focal point approximately 10 ns before the defined time zero (0 ns), initiated by the arrival of the focused laser pulse in the supercritical medium. The plasma expands predominantly in the direction opposite to the laser propagation, within the focusing envelope indicated by the dashed lines. The emission intensity reaches its peak at 0 ns, marking the end of the initial expansion phase. Following this, the plasma gradually relaxes and dissipates. (**d**) Time-resolved optical emission spectra captured during the relaxation phase. The measured continuum emission is well fitted by blackbody radiation curves (dashed lines), indicating local thermodynamic equilibrium (LTE) conditions in the dense plasma.

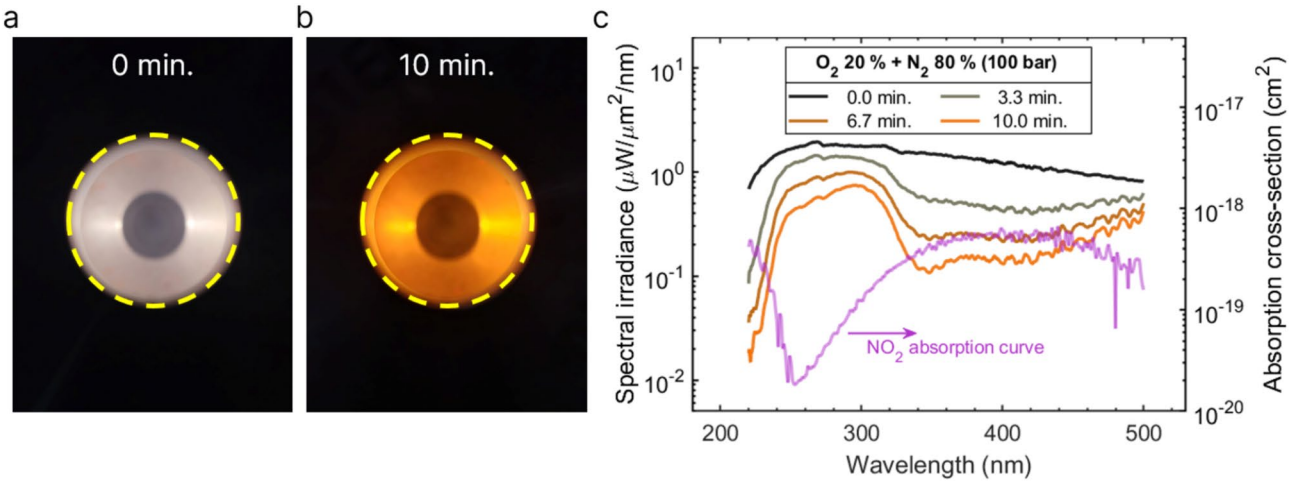

Fig. 2. NO_2 formation via plasma-induced chemical reactions. (**a**, **b**) Images of inside the high-pressure chamber (filled with a 100 bar mixture of N_2 and O_2). Panel a shows the chamber at the initial state (0 min), while panel b shows its appearance after 10 min of continuous plasma generation. A distinct reddish-brown coloration appears, indicating the formation of NO_2. The dashed yellow outlines the window's clear aperture, and the black circular area within the window corresponds to the gas inlet located on the opposite side of the chamber. (**c**) Time-resolved optical emission spectra acquired during plasma generation. Over time, the overall emission intensity decreases due to absorption by the generated NO_2. The purple curve represents the absorption cross section of NO_2[21,22], which corresponds closely to the observed absorption features.

$$\ln\left(\frac{I_0}{I}\right) = \sigma(\lambda) \cdot n \cdot l, \tag{1}$$

where I_0 and I denote the spectral intensities before and after absorption, respectively; $\sigma(\lambda)$ is the absorption cross section at wavelength λ; n is the number density of NO_2; and l is the optical path length through the absorbing medium. Since the plasma is generated at the center of the chamber, the effective path length l is taken as half the chamber width, around 3.5 cm. The absorption cross-section data $\sigma(\lambda)$ are well-documented, and the time-dependent spectral intensities I_0/I are measured experimentally. Using these values, the NO_2 number density n is calculated. To minimize uncertainties caused by the wavelength dependence of $\sigma(\lambda)$, the estimation is performed near 400 nm, where the cross-section curve is relatively flat. At this wavelength, NO_2 exhibits a dominant absorption cross-section compared to all other potentially coexisting species. In particular, NO, N_2O, and O_3 are known to exhibit strong absorption primarily in the UV region, but their absorption cross-sections decrease rapidly and become negligible in the visible regime[22,23]. Therefore, the observed absorbance can be attributed almost exclusively to NO_2, and the contribution from other species can be safely ignored. Figure 3 shows the calculated NO_2 density as a function of time. Considering that the vertical axis is plotted on a logarithmic scale, it is evident that most of the NO_2 generation occurs during the early stage of the repetitive (2 Hz) plasma generations, with the growth rate gradually slowing down over time. The observed saturation in NO_2 accumulation suggests the emergence of a dynamic balance between formation and decomposition processes. In the high-energy plasma environment, NO_2 molecules may undergo secondary dissociation through electron impact[24–26] or photo-induced pathways[27,28]. As these backward reactions become more prominent over time, the net production rate of NO_2 decreases, leading to the observed saturation behavior. To confirm that the presence of NO_2 does not significantly alter the optical properties of the plasma used as a light source, we repeated the absorption measurement using an external collimated LED beam. The resulting NO_2 density, shown in Supplementary Figure 1, is consistent with the values obtained from plasma-based measurements, supporting the validity of our diagnostic approach.

The estimated NO_2 number density reaches approximately 1×10^{18} cm^{-3}, as determined from the absorption analysis. This corresponds to an NO_2 concentration of approximately 500 ppm within the 100 bar high-pressure chamber. Given the laser repetition rate of 2 Hz and a total measurement time of 10 min, approximately 1200 laser pulses are delivered during the experiment. Each optical emission spectrum is acquired by averaging 20 consecutive pulses to ensure a sufficient signal-to-noise ratio. Due to the low viscosity and high diffusivity of the supercritical fluid, the generated NO_2 molecules are expected to be uniformly distributed throughout the chamber. Considering the chamber volume of 50 cm^3, the total number of NO_2 molecules is estimated to be 5×10^{19}, corresponding to approximately 4×10^{16} molecules produced with each pulse. Given that the bond dissociation energy of the N–O bond in NO_2 is approximately 3.2 eV[26,29,30], the chemical energy of NO_2 formation per pulse is about $4 \times 10^{16} \times 3.2$ eV $\times 1.6 \times 10^{-19}$ J/eV ≈ 20 mJ. Compared to the incident laser pulse energy is 620 mJ, the overall energy efficiency is on the order of 3%. To more accurately evaluate the energy consumption, it is important to account for the actual laser energy deposited into the plasma. Approximately 14% of the initial energy is reflected at the sapphire window, and 50 mJ is transmitted without contributing to

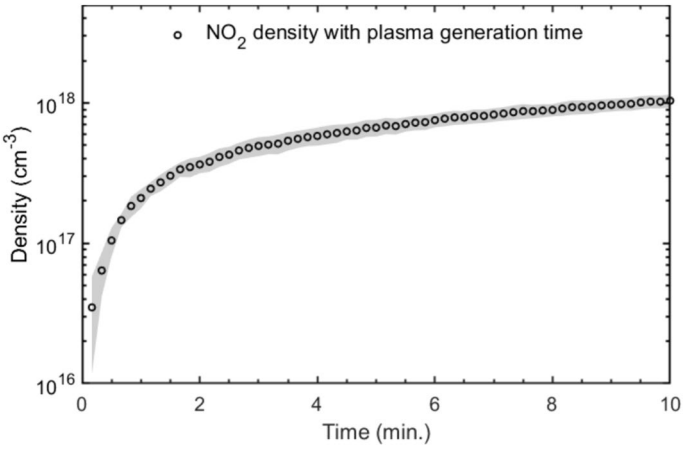

Fig. 3. Temporal evolution of the estimated NO_2 density, derived from the time-resolved absorption spectra. A rapid increase in NO_2 density is observed in the early stage of plasma generation at a repetition rate of 2 Hz. The NO_2 density gradually saturates over time. After 10 minutes, the NO_2 density reaches approximately 1.0 $\times 10^{18}$ cm^{-3}, which corresponds to about 1/2000 of the total particle density inside the 100 bar high-pressure chamber. The shaded area represents the standard deviation from five repeated measurements.

plasma generation. Accordingly, the effective energy input to the plasma is estimated to be around 480 mJ. The energy consumption for NO_2 produced per pulse is given by

$$\begin{aligned}\text{Energy consumption per mol} &= \frac{\varepsilon\,[\text{J/pulse}]}{\text{mol of } NO_2 \text{ produced per pulse } [mol/pulse]} \\ &= \frac{0.48}{4\times 10^{16}/(6.02\times 10^{23})}[\text{J/mol}] \approx 7[\text{MJ/mol}].\end{aligned} \tag{2}$$

Although this is less efficient than the Ostwald process (0.6 MJ/mol)[1], it is comparable to other plasma-based NO_x synthesis methods[31,32] or even lower energy consumption relative to dielectric barrier discharge (DBD) reactors (16–540 MJ/mol)[32–35]. Importantly, employing pulsed lasers allows for precise manipulation of the chemical reaction and the production of NO_2 by adjusting the laser pulse energy and repetition rate, providing a degree of control that is not easily attainable with traditional plasma systems. The ability to induce direct NO_2 formation through transient, localized plasma in a dense supercritical fluid environment underscores the potential of this system for cumulative, high-efficiency chemical processing under high-repetition operation.

The use of a supercritical N_2-O_2 mixture provides several advantages for plasma formation and subsequent NO_2 production. At higher pressures, the threshold laser energy required to initiate plasma formation is reduced, allowing more efficient plasma generation[36]. In addition, the plasma volume increases significantly with pressure, which expands the region where reactive species are generated. These factors directly contribute to the enhanced chemical yield observed under supercritical fluid conditions. Figure 4 shows comparative measurements between gas phase (10 bar) and supercritical fluid (100 bar) conditions, showing a notable increase in NO_2 production at supercritical pressure. At 10 bar, the NO_2 production was consistently less than at 100 bar, showing nearly a twofold variation after 10 min. Although the plasma lifetime at 10 bar is longer due to the lower collision rate, the supercritical fluid at high pressure produces significantly more NO_2, indicating the advantage of the supercritical fluid in enhancing NO_2 formation. Note that the two pressure points are representative of subcritical and supercritical conditions, respectively. An extensive set of experiments at intermediate pressures and different temperatures would be necessary to understand the mechanism of enhancement of plasma chemistry reactions in supercritical fluid states compared to subcritical states.

Parametric investigation of NO^2 formation mechanisms

The formation of NO_2 in the supercritical mixture of N_2 and O_2 originates not from the laser pulse itself, but from the chemical reactions triggered by the laser-produced plasma. Although the photon energy of the laser is insufficient to directly dissociate the strongly bonded N_2 or O_2 molecules, the plasma environment facilitates the generation of molecular ions such as N_2^+, which dissociate more easily than neutral molecules and act as crucial intermediates for NO_2 formation. While the laser pulse does not directly induce the chemical reaction, its energy significantly affects the plasma volume (Fig. 5a). As the laser pulse propagates toward the focal point, its intensity increases, causing pre-ionization and molecular excitations via multiphoton processes. Plasma ignition begins at the focal point and expands in the form of an ionization wave into the region where the pre-ionized electrons and excited molecules exist. A higher pulse energy results in sufficient pre-ionized electrons, enabling plasma expansion over a larger volume. Since the plasma serves as the reactive environment for NO_2 formation to occur, a clear correlation between plasma volume and NO_2 density is observed (Fig. 5b). At pulse energies below 100 mJ, both the plasma volume and resulting NO_2 density decrease sharply. In addition to plasma volume, plasma lifetime also influences the availability of reactive species needed for NO_2 synthesis.

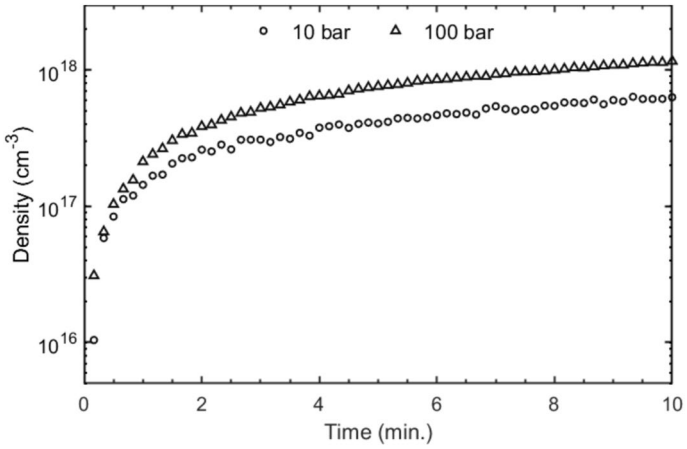

Fig. 4. Temporal evolution of NO_2 density measured at 10 bar (circle) and 100 bar (triangle). The NO_2 yield at 100 bar, which corresponds to the supercritical regime, is approximately twice that at 10 bar. This result indicates that the high-pressure supercritical fluid significantly enhances plasma-based chemical reactions.

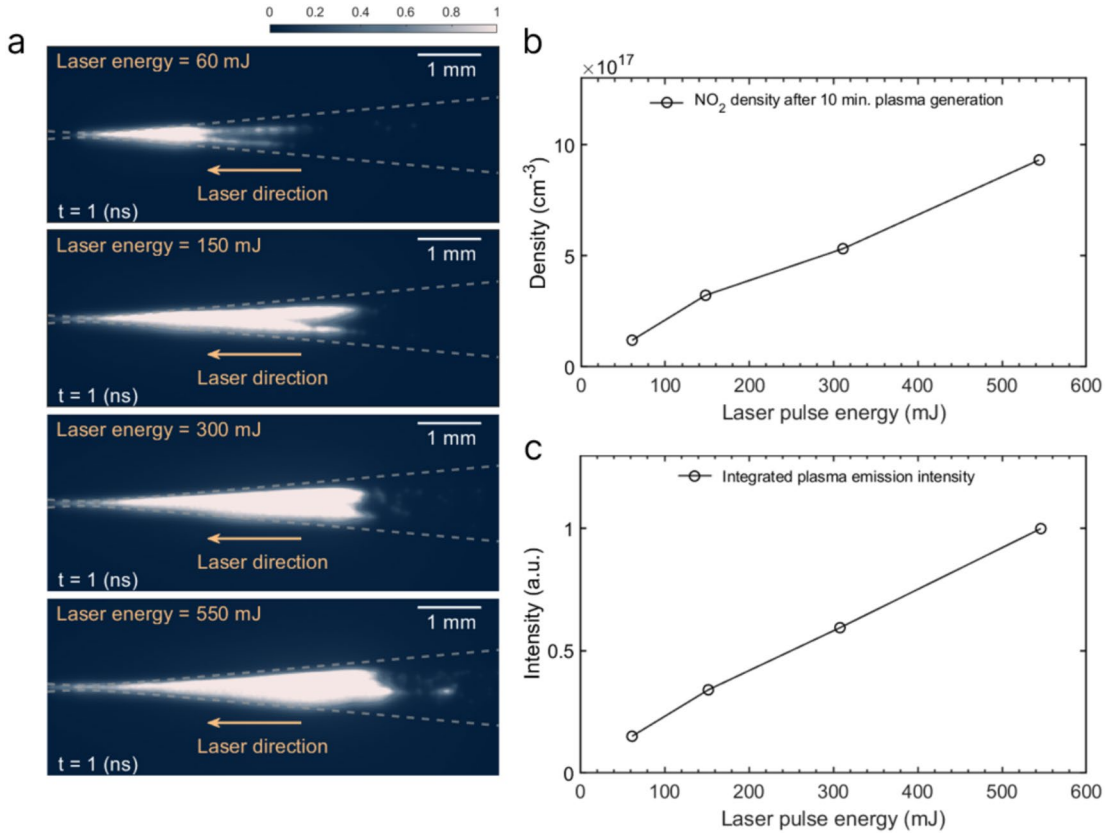

Fig. 5. Effect of laser pulse energy on plasma formation and NO_2 production. (**a**) Plasma images captured at varying laser pulse energies, illustrating the increase in plasma volume with increasing energy. All images are normalized to their respective maximum intensity for visual clarity. (**b**) Measured NO_2 density as a function of laser pulse energy. (**c**) Integrated optical emission intensity over time for different laser energies. This reflects the combined effects of plasma volume and lifetime, and shows good agreement with the NO_2 yield trend.

This trend is supported by the integrated plasma intensity, which reflects the trend in NO_2 yield, as shown in Fig. 5c. Below a certain energy threshold, both plasma volume and lifetime diminish sharply, resulting in a notable drop in NO_2 formation efficiency. In addition to the optical diagnostics presented here, the NO_2 concentration is independently verified using a commercial gas analyzer (TESTO 350), with measurements performed across

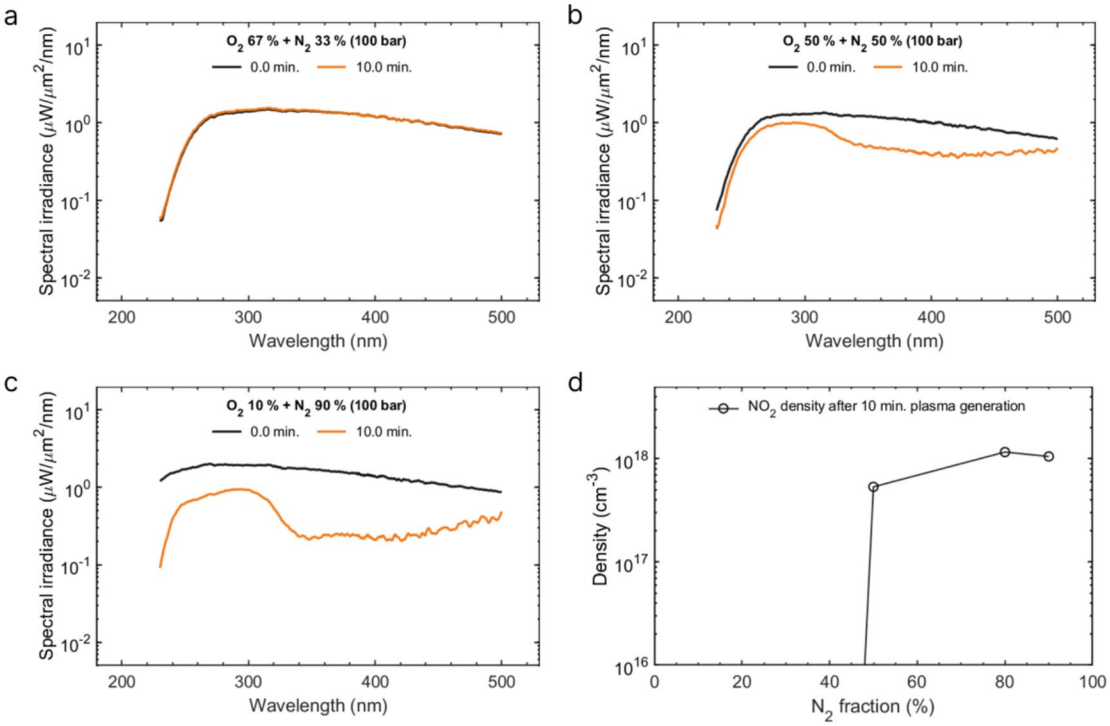

Fig. 6. Effect of gas composition on plasma-induced NO_2 formation. (**a**–**c**) Optical emission spectra measured in 100 bar supercritical mixtures with N_2 fractions of 33%, 50%, and 90%, respectively. At 33% N_2, no spectral change is observed after 10 min, indicating negligible NO_2 formation. At 50% N_2, a slight decrease in emission intensity suggests limited NO_2 production. At 90% N_2, strong absorption features emerge after 10 minutes, consistent with significant NO_2 generation. (**d**) Final NO_2 number densities for N_2 fractions of 33%, 50%, 80%, and 90% show a sharp increase above 50% N_2, highlighting the critical role of nitrogen availability in NO_2 formation.

varying laser pulse energies (see n Fig. 2). This complementary method confirms the reliability of our optical quantification of NO_2 yield.

Discussion

Another intriguing observation is that the amount of NO_2 varies significantly depending on the fraction of N_2 and O_2 in the supercritical fluid (Fig. 6). NO_2 production relies on the availability of nitrogen radicals, which are primarily generated through the dissociation of N_2 molecules. In high-temperature, high-electron-density plasma environments, N_2 can dissociate via electron impact, dissociative excitation, and dissociative ionization, producing reactive nitrogen atoms that readily react with O and O_2 to form NO or NO_2. Thus, maintaining a sufficient concentration of N_2 in the gas mixture is essential for sustaining the supply of N radicals. Figure 6d shows that increasing the proportion of O_2 leads to a decrease in NO_2 formation. This trend suggests that the dissociation of N_2, rather than the abundance of O_2, is the rate-limiting factor in plasma-driven NO_2 synthesis. When the O_2 fraction exceeds 50%, NO_2 generation is almost entirely suppressed. This suppression can be attributed to the competing effects of O_2 during plasma generation and relaxation process. Molecular oxygen introduces alternative energy loss pathways through excitation and ionization, diverting energy from N_2 dissociation. As a result, the generation of nitrogen radicals is significantly hindered in O_2-rich mixtures, limiting the formation of NO and NO_2.

Conclusion

We have demonstrated a novel plasma-based method for the direct synthesis of nitrogen dioxide (NO_2) from compressed mixtures of nitrogen and oxygen in a high-pressure supercritical fluid environment. Without relying on ammonia or multistep catalytic processes (i.e., the Haber-Bosch and Ostwald processes), our approach enables one-step conversion of air-like gases into NO_2 using focused laser pulses to generate high-energy-density plasma. Since this study compares only a single subcritical and a single supercritical pressure point, further studies involving a wider range of pressures near the critical point will be needed to fully elucidate the unique influence of the supercritical fluid state on NO_2 formation. However, this method provides a promising alternative to conventional ammonia-based routes for producing nitrogen oxides and related compounds.

Beyond its simplicity and compactness, this technique has particular relevance for applications in space exploration and remote environments, where the ability to generate essential chemical species, such as NO_2 and nitric acid (HNO_3), directly from stored or ambient gases is highly advantageous. Our findings lay the

groundwork for developing decentralized, on-demand systems for nitrogen compound production, with potential implications in closed-loop life support systems and in-situ resource utilization.

Methods

Preparation of high-pressure supercritical environments

A high-pressure supercritical fluid is prepared using a mixed gas composed of nitrogen (N_2) and oxygen (O_2) at an 80:20 ratio. The compressor operates at an input pressure of approximately 6 bar and contains two pistons connected to a rotating motor. The first piston performs initial compression, and the second piston further compresses the gas before ejecting it. A check valve installed at the piston outlet opens at 300 bar. The compressed gas is delivered to the high-pressure chamber through quick connectors and flexible hoses (Swagelok SS-QF4 and SS-FX4TA4TA4).

The internal pressure of the system is monitored in real time using a pressure gauge and a pressure sensor (Keller LEO2 and Tival TST-20). A target pressure of 100 bar in the experiments exceeds both the critical pressure of nitrogen (34 bar) and oxygen (50 bar). The experiments were conducted at room temperature (295 K), which is well above the critical temperatures of nitrogen (126.2 K) and oxygen (154.6 K). Hence, under the given pressure and temperature conditions, a supercritical fluid is ensured. Once the target pressure is reached, the compressor is stopped, and the valve to the high-pressure chamber is closed to isolate the high-pressure chamber.

The high-pressure chamber used in this study is a cube-shaped cell (65 mm per side) constructed from SUS304 stainless steel. Sapphire windows (Rayotek) are mounted on five of the six faces to allow optical access, while the remaining face is connected to a hose for the introduction of compressed gas from an external compressor. Each sapphire window has a thickness of approximately 4 mm and provides a clear aperture of 11 mm in diameter. Due to the depth of the sapphire windows, the total optical path length of photons inside the chamber is slightly longer than half the chamber length, measuring approximately 3.5 cm.

According to Lee et al.[37], the compression and expansion process involved in filling the chamber generates liquid-like particles that persist for extended durations under high-pressure conditions ($\sim$ hour). To minimize the effects of such inhomogeneities (e.g., droplets or clusters), a laser pulse for plasma generation is applied approximately one hour after reaching the target pressure. The amount of NO_2 produced is then measured.

In experiments comparing NO_2 generation at various N_2 fractions, pure N_2 and O_2 gases are combined directly via the compressor. Mixtures containing 33%, 50%, and 90% N_2 by volume are created and pressurized using the identical method, and the resulting NO_2 yields are analyzed for comparison.

Optical emission spectroscopy setup and timing

The experimental setup is identical to that reported in previous work [20]. A brief summary is provided below for clarity.

A Q-switched Nd:YAG laser (Quentel, Brilliant B, 1064 nm, 6 ns, 650 mJ, 2 Hz repetition rate) was used, with a beam diameter of 9 mm. The beam was focused using a plano-convex lens (f = 50 mm), resulting in an estimated focal spot diameter of $\sim$ 50 um. The photons emitted from the laser-produced plasma provide valuable information about thermodynamic properties of plasmas, such as electron density and electron temperature. At the same time, the plasma emission serves as a broadband light source for absorption measurements. Due to the high electron density, the plasma has a transient emission lifetime. To capture this short-lived emission, an ICCD camera (Teledyne Princeton Instruments PI-MAX4) with a nanosecond-scale gate width is used. The light emission from the plasma is collected by a lens and an optical fiber (Thorlabs, NA: 0.22, core diameter: 600 μm) with collection area: $\sim$ 0.43 mm^2. The light is guided to Czerny-Tuner type monochromator (Teledyne Princeton Instruments) which has a focal length of 300 mm and 150 groove/mm grating.

For quantitative analysis of emission intensity, an intensity calibration source (Ocean Optics, DH-3 Plus) is employed. Wavelength-dependent responses of the optical system—such as the transmission of the optical fiber, the spectral response of the monochromator, and the quantum efficiency of the ICCD camera—are all accounted for during calibration.

In the measurements shown in Fig. 1, plasma spectra are recorded at two different delay times (1 ns and 100 ns) after plasma generation, with a gate width of 3 ns. Each spectrum is obtained by averaging 20 laser shots. The continuum emission is well fitted using a blackbody curve described by the the Planck function,

$$I_\lambda = \varepsilon \frac{2\pi hc^2}{\lambda^5\{\exp(hc/\lambda k_B T) - 1\}}, \tag{3}$$

where h, c, λ, k_B, and T are the Planck constant, the speed of light, the wavelength, the Boltzmann constant, and the blackbody temperature, respectively. The emissivity ε ranges between 0 and 1, and shows how closely the plasma resembles an ideal blackbody. The emissivity values are approximately 0.8 at 1 ns and 0.07 at 100 ns. The same plasma emission spectra are also used as the light source for absorption measurements related to NO_2 formation. In these cases, spectra acquired at a delay time of 1 ns, corresponding to the strongest plasma emission, are analyzed. Figures 2c and 6a–c show the spectrum change over time, all acquired at a delay of 1 ns with a gate width of 3 ns.

Data availability

All relevant data supporting this study are available from the authors (J.L. and G.Y.) upon reasonable request.

Received: 21 May 2025; Accepted: 20 September 2025

Published online: 27 October 2025

References

1. Rouwenhorst, K. H. R., Jardali, F., Bogaerts, A. & Lefferts, L. From the birkeland–eyde process towards energy-efficient plasma-based nox synthesis: A techno-economic analysis. *Energy Environ. Sci.* **14**, 2520–2534. https://doi.org/10.1039/D0EE03763J (2021).
2. Atkinson, R. Atmospheric chemistry of vocs and nox. *Atmos. Environ.* **34**, 2063–2101. https://doi.org/10.1016/S1352-2310(99)00460-4 (2000).
3. Finlayson-Pitts, B. J. & Pitts, J. N. *Chemistry of the Upper and Lower Atmosphere: Theory, Experiments, and Applications* (Elsevier, 1999).
4. P'erez-Ramírez, J., Kondratenko, E. V., Novell-Leruth, G. & Ricart, J. M. Mechanism of ammonia oxidation over pgm (pt, pd, rh) wires by temporal analysis of products and density functional theory. *J. Cataly.* **261**, 217–223. https://doi.org/10.1016/j.jcat.2008.11.018 (2009).
5. Hannevold, L., Nilsen, O., Kjekshus, A. & Fjellvåg, H. Reconstruction of platinum–rhodium catalysts during oxidation of ammonia. *Appl. Cataly. A General* **284**, 163–176. https://doi.org/10.1016/j.apcata.2005.01.033 (2005).
6. Grande, C. A. et al. Process intensification in nitric acid plants by catalytic oxidation of nitric oxide. *Ind. Eng. Chem. Res.* **57**, 10180–10186. https://doi.org/10.1021/acs.iecr.8b01483 (2018).
7. Gopakumar, J. et al. Ostwald process intensification by catalytic oxidation of nitric oxide. *Ind. Eng. Chem. Res.* **10**, 2197–2211. https://doi.org/10.1021/acsomega.4c09111 (2025).
8. Ma, H. & Schneider, W. F. Dft and microkinetic comparison of pt, pd and rh-catalyzed ammonia oxidation. *J. Catal.* **383**, 322–330. https://doi.org/10.1016/j.jcat.2020.01.029 (2020).
9. Novell-Leruth, G., Ricart, J. M. & Pérez-Ramírez, J. Pt(100)-catalyzed ammonia oxidation studied by dft: Mechanism and microkinetics. *J. Phys. Chem. C* **112**, 13554–13562. https://doi.org/10.1021/jp802489y (2008).
10. Hauthal, W. H. Advances with supercritical fluids [review]. *Chemosphere* **43**, 123–135. https://doi.org/10.1016/S0045-6535(00)00332-5 (2001).
11. Uwineza, P. A. & Waśkiewicz, A. Recent advances in supercritical fluid extraction of natural bioactive compounds from natural plant materials. *Molecules* **25**, 3847. https://doi.org/10.3390/molecules25173847 (2020).
12. Bolmatov, D., Brazhkin, V. V. & Trachenko, K. Thermodynamic behaviour of supercritical matter. *Nat. Commun.* **4**, 2331. https://doi.org/10.1038/ncomms3331 (2013).
13. Manjare, S. D. & Dhingra, K. Supercritical fluids in separation and purification: A review. *Mater. Sci. Energy Technol.* **2**, 463–484. https://doi.org/10.1016/j.mset.2019.04.005 (2019).
14. Ye, X. R., Lin, Y. & Wai, C. M. Decorating catalytic palladium nanoparticles on carbon nanotubes in supercritical carbon dioxide. *Chem. Commun.* **5**, 642–643. https://doi.org/10.1039/B211350C (2003).
15. Hiramatsu, M. & Hori, M. Preparation of dispersed platinum nanoparticles on a carbon nanostructured surface using supercritical fluid chemical deposition. *Materials* **3**, 1559–1572. https://doi.org/10.3390/ma3031559 (2010).
16. Zhang, Y. & Erkey, C. Preparation of supported metallic nanoparticles using supercritical fluids: A review. *J. Supercritical Fluids* **38**, 252–267. https://doi.org/10.1016/j.supflu.2006.03.021 (2006).
17. Byrappa, K., Ohara, S. & Adschiri, T. Nanoparticles synthesis using supercritical fluid technology—Towards biomedical applications. *Adv. Drug Deliv. Rev.* **60**, 299–327. https://doi.org/10.1016/j.addr.2007.09.001 (2008).
18. Oshima, F., Stauss, S., Ishii, C., Pai, D. Z. & Terashima, K. Plasma microreactor in supercritical xenon and its application to diamondoid synthesis. *J. Phys. D Appl. Phys.* **45**, 402003. https://doi.org/10.1088/0022-3727/45/40/402003 (2012).
19. Stauss, S., Muneoka, H., Urabe, K. & Terashima, K. Review of electric discharge microplasmas generated in highly fluctuating fluids: Characteristics and application to nanomaterials synthesis. *Phys. Plasmas* **22**, 057103. https://doi.org/10.1063/1.4921145 (2015).
20. Lee, S., Lee, J., Yoon, Y. D., Kim, D. E. & Yun, G. Characterization of strongly coupled plasmas produced in argon supercritical fluids. *Plasma Phys. Controlled Fusion* **64**, 095010. https://doi.org/10.1088/1361-6587/ac7ee8 (2022).
21. Bass, A., Ledford, A. & Laufer, A. Extinction coefficients of NO2 and N2O4. *J. Res. Natl. Bur. Stand. Sect. A* **80**(2), 143. https://doi.org/10.6028/jres.080A.017 (1976).
22. Huh, S.-C. et al. Individual quantification of ozone and reactive nitrogen species in mixtures by broadband UV–Visible absorption spectra deconvolution. *Plasma Sources Sci. Technol.* **33**, 075007. https://doi.org/10.1088/1361-6595/ad5ebb (2024).
23. Brion, J. et al. Absorption spectra measurements for the ozone molecule in the 350–830 nm region. *J. Atmos. Chem.* **30**, 291–299. https://doi.org/10.1023/A:1006036924364 (1998).
24. Abouaf, R., Paineau, R. & Fiquet-Fayard, F. Dissociative attachment in NO_2 and CO_2. *J. Phys. B Atomic Mol. Phys.* **9**, 303. https://doi.org/10.1088/0022-3700/9/2/017 (1976).
25. Gope, K., Tadsare, V., Prabhudesai, V. S. & Krishnakumar, E. Production of electronically excited no via dea to NO_2. *Eur. Phys. J. D* **71**, 323. https://doi.org/10.1140/epjd/e2017-80539-1 (2017).
26. Song, M.-Y. et al. Cross sections for electron collisions with NO, N_2O, and NO_2. *J. Phys. Chem. Ref. Data* **48**, 043104. https://doi.org/10.1063/1.5114722 (2019).
27. Wilkinson, I., Garcia, I. A., Whitaker, B. J., Hamard, J.-B. & Blanchet, V. The photodissociation of NO_2 by visible and ultraviolet light. *Phys. Chem. Chem. Phys.* **12**, 15766–15779. https://doi.org/10.1039/C0CP01551B (2010).
28. Zhang, Z. et al. Slice imaging study of no2 photodissociation via the 12b2 and 22b2 states: the NO($X^2\Pi$) + O(^3PJ) product channel. *Phys. Chem. Chem. Phys.* **25**, 16872–16880. https://doi.org/10.1039/D3CP00420A (2023).
29. Haynes, W. M. *CRC Handbook of Chemistry and Physics* (sCRC Press, 2016).
30. Bach, R. D. & Schlegel, H. B. The bond dissociation energy of the N–O bond. *J. Phys. Chem. A* **125**, 5014–5021. https://doi.org/10.1021/acs.jpca.1c02741 (2021).
31. Vervloessem, E., Gorbanev, Y., Nikiforov, A., Geyter, N. & Bogaerts, A. Sustainable NO_x production from air in pulsed plasma: Elucidating the chemistry behind the low energy consumption. *Green Chem.* **24**, 916–929. https://doi.org/10.1039/D1GC02762J (2022).
32. Rouwenhorst, K. H. R., Tabak, S. & Lefferts, L. Improving the energy yield of plasma-based NO_x synthesis with in situ adsorption. *React. Chem. Eng.* **9**, 528–531. https://doi.org/10.1039/D3RE00593C (2024).
33. Pei, X., Gidon, D., Yang, Y.-J., Xiong, Z. & Graves, D. B. Reducing energy cost of NO_x production in air plasmas. *Chem. Eng. J.* **362**, 217–228. https://doi.org/10.1016/j.cej.2019.01.011 (2019).
34. Patil, B. et al. Low temperature plasma-catalytic NO_x synthesis in a packed DBD reactor: Effect of support materials and supported active metal oxides. *Appl. Catal. B Environ.* **194**, 123–133. https://doi.org/10.1016/j.apcatb.2016.04.055 (2016).
35. Ma, Y., Wang, Y., Harding, J. & Tu, X. Plasma-enhanced N_2 fixation in a dielectric barrier discharge reactor: Effect of packing materials. *Plasma Sources Sci. Technol.* **30**, 105002–105013. https://doi.org/10.1088/1361-6595/ac2412 (2021).
36. R. G. Meyerand, J. & Haught, A. F. Gas breakdown at optical frequencies. *Phys. Rev. Lett.* **11** (1963).
37. Lee, S. et al. Quasi-equilibrium phase coexistence in single component supercritical fluids. *Nat. Commun.* https://doi.org/10.1038/s41467-021-24895-y (2021).

Acknowledgements
This work was supported by the National Research Foundation of Korea (NRF) grant funded by the Ministry of Science and ICT (RS-2024-00349684) and supported by the Glocal University 30 project funded by the Ministry of Education. G.Y. thanks Prof. Yung Kyun Noh at the Center for AI and Natural Sciences, Korea Institute for Advanced Study (KIAS), for fruitful discussions on the experimental results and modeling of plasma chemistry.

Author contributions
G.Y. proposed the original idea and conceived the project. J.L. designed the laser plasma experiments under high-pressure conditions. J.L. and K.C. conducted time-resolved imaging and OES experiments to investigate the characteristics of dense plasmas generated in nitrogen and oxygen supercritical fluid mixtures. J.L. carried out the data processing and analysis. J.L. and S.L. analyzed the amount of generated NO2. J.L. wrote the manuscript. G.Y. supervised the project. All authors contributed significantly to the discussion of the results. All authors reviewed the manuscript.

Declarations

Competing interests
The authors declare no competing interests.

Additional information
Supplementary Information The online version contains supplementary material available at https://doi.org/10.1038/s41598-025-21381-z.

Correspondence and requests for materials should be addressed to G.Y.

Reprints and permissions information is available at www.nature.com/reprints.

Publisher's note Springer Nature remains neutral with regard to jurisdictional claims in published maps and institutional affiliations.